Rapid Communications in Mass Spectrometry, research article

Cite this article as:
Klenner F, Postberg F, Hillier J, et al. Analogue spectra for impact ionization mass spectra of water ice grains obtained at different impact speeds in space. *Rapid Commun Mass Spectrom.* 2019;**33**(22):1751-1760. doi: 10.1002/rcm.8518

Analogue spectra for impact ionization mass spectra of water ice grains obtained at different impact speeds in space

Fabian Klenner[1,2*], Frank Postberg[1,2], Jon Hillier[1], Nozair Khawaja[1,2], René Reviol[1,2], Ralf Srama[3], Bernd Abel[4,5], Ferdinand Stolz[4,5] & Sascha Kempf[6]

[1]Institut für Geologische Wissenschaften, Freie Universität Berlin, Malteserstraße 74-100, D-12249 Berlin, Germany

[2]Institut für Geowissenschaften, Ruprecht-Karls-Universität Heidelberg, Im Neuenheimer Feld 234-236, D-69120 Heidelberg, Germany

[3]Institut für Raumfahrtsysteme, Universität Stuttgart, Pfaffenwaldring 29, D-70569 Stuttgart, Germany

[4]Leibniz-Institut für Oberflächenmodifizierung, Permoserstraße 15, D-04318 Leipzig, Germany

[5]Wilhelm-Ostwald-Institut für Physikalische und Theoretische Chemie, Universität Leipzig, Linnéstraße 2, D-04103 Leipzig, Germany

[6]Laboratory for Atmospheric and Space Physics, University of Colorado, 1234 Innovation Dr, Boulder, CO 80303-7814, USA

[*]Corresponding author e-mail: f.klenner@fu-berlin.de

Received: 2019 February 22. Accepted for publication: 2019 June 30.

Abstract

RATIONALE: Detecting ice grains with impact ionization mass spectrometers in space provides information about the ice grains' compositions and their sources. Depending on the impact speeds of the ice grains onto the metal target of a mass spectrometer,

ionization conditions can vary substantially, resulting in changes to the appearance of the resulting mass spectra.

METHODS: Here we accurately reproduce mass spectra of water ice grains, recorded with the Cosmic Dust Analyzer (CDA) on board the Cassini spacecraft at typical impact speeds ranging between 4 km/s to 21 km/s, with a laboratory analogue experiment. In this Laser-Induced Liquid Beam Ion Desorption (LILBID) approach, a µm-sized liquid water beam is irradiated with a pulsed infrared laser, desorbing charged analyte and solvent aggregates and isolated ions, which are subsequently analyzed in a time of flight mass spectrometer (TOF-MS).

RESULTS: We show that our analogue experiment can reproduce impact ionization mass spectra of ice grains obtained over a wide range of impact speeds, aiding the quantitative analyses of mass spectra from space.

CONCLUSIONS: Spectra libraries created with the LILBID experiment will be a vital tool for inferring the composition of ice grains from mass spectra recorded by both past and future impact ionization mass spectrometers (e.g. the SUrface Dust Analyzer (SUDA) onboard NASA's Europa Clipper Mission or detectors on a future Enceladus Mission).

Keywords: Cassini, Enceladus, Ice analogue, Mass spectrometry, Ocean worlds

1 Introduction

Dust detectors have played an important role in spacecraft payloads since at least the Pioneer 8 mission, probing in situ not only mineral dust but also ice grains.[1-6] Later 'active' detectors produce information about the grains' compositions and, therefore, provide insights into the compositions of the sources from which the grains were emitted.[7-15] Ice grains striking a detector's target plate, at speeds above approximately 1 km/s, form impact clouds containing ions and electrons, together with neutral atoms, molecules and macroscopic fragments. Charged particles (electrons, atomic ions and molecular ions) are, polarity dependent, separated and accelerated through a strong electric field towards a detector. Depending on the complexity of the mass spectrometer used, they may pass through either a field-free (or near field-free in the case of CDA) or a reflectron[16] region. The ions' arrival times are proportional to their mass to charge ratios, thus forming time of flight mass spectra. In contrast to

spaceborne neutral gas mass spectrometers, where ionization occurs in a controlled way using electrons with well-constrained energies[17-19], impact ionization relies on the kinetic energy delivered by the impact. The impact speeds of ice grains in space may vary drastically (<5 to >20 km/s), resulting in variations in the energy available for disrupting and ionizing molecular and atomic species. The resulting mass spectra can therefore appear very different, even if the grains are identically composed, with higher mass water cluster ions decreasing in abundance as the impact energy increases. Laboratory analogue experiments in which water ice targets are exposed to high velocity dust particles, producing these water clusters of the form $[(H_2O)_nH_3O]^+$ show similar variations, with fewer larger (higher n) clusters surviving as the impact velocity increases.[20] The reduction in high mass molecular clusters is primarily linked to the change in impact plasma conditions, with more destructive collisions and a shortening of the timescales over which clustering can occur, with higher energy, faster expanding clouds experiencing longer clustering mean free paths over shorter times, prior to acceleration and detection.

In contrast to siliceous, metallic, or organic grains, micron and sub-micron sized ice grains can currently not be accelerated in an electrostatic dust accelerator facility to relevant speeds.[21-27] Previous studies[12,28] have shown that CDA impact ionization mass spectra of ice grains with varying minor compositional differences can be reproduced with laboratory analogue experiments in which a pulsed infrared laser intercepts an ultra-thin water beam or water droplets. However, those studies did not consider the role impact speed plays in determining spectral appearance. The collisional behavior of ions and neutrals within the expanding plasma cloud, leading to recombination, ionization, fragmentation and/or clustering, is a function of the impact cloud expansion speed, energetics and the number density of interacting species within it.[29] Typically, four factors determine the initial composition and dynamics of the cloud of ions and neutrals generated during an impact: impact speed, particle mass, and particle and target composition. Although particle mass also influences the total amount of charge generated by an impact[30], the clearly dominant factor here is impact speed (total impact charge typically scales proportionally to $m^{\alpha}v^{\beta}$, with α typically near one and β varying between approximately 3 and 5 with target and projectile composition[27,30]). Impact ionization also primarily occurs at shock fronts, for which the controlling factor is energy per unit mass, and hence is impact speed dependent. To improve the compositional analyses of ice grains and their planetary sources an analogue experiment should be able to simulate the varying ionization and clustering conditions that occur at different impact speeds.

Building on the work of Postberg et al. 2009a[12], here we adapt laser desorption analogue experiments to mimic a wide range of feasible impact speeds, establishing an experimental methodology to predict and reproduce mass spectra generated by ice grains in the future. This will improve quantitative compositional analysis of mass spectra produced by impact ionization mass spectrometers on board not only Cassini[31], but also on future spacecraft intended to investigate icy moons, such as the Europa Clipper and Enceladus missions.[32-36]

2 Experimental

Scientific approach

Spaceborne impact ionization mass spectrometers form projectile ions from micrometer-sized ice grains as the grains impact onto targets (Figure 1 A). In the case of Cassini's CDA, ice particles impinge onto a rhodium target, vaporizing and ionizing speed-dependent fractions of both projectile and target. At the low impact speeds considered here, there is no evidence of the generation of multiply charged ions during this process. A 1000 V potential difference, between the impact target (+1000 V) and a grid held at 0 V, approximately 3 mm in front of it, accelerates cations through a near-drift region towards an ion detector, the multiplier, at a distance of 0.23 m. A series of three concentric grids, separated by 0.005 m and held at ~ -350 V, ~0.03 m in front of the multiplier, provide only marginal further ion focusing and acceleration. After passing through the grids, the central of which is connected to a charge amplifier and recorder to produce the QI signal[31], the ions experience a post acceleration towards the multiplier front electrode, held at ~ -2750 V (Figure 1 C). The ice grains' impact speeds may be determined not only by the rise times of the charge signals on the target and/or the ion grids of CDA[31], and/or via spectral appearance (i.e. a decrease in cluster size, appearance of target material ions, production of ions with high ionization energies[37,38]), but also through dynamical considerations. In this latter technique, the known position of the spacecraft when individual E ring ice grains are detected can be used to estimate the speed of the particle in a circular orbit passing through this point. After subtraction of the known speed of the spacecraft, the likely impact speed for the particle can be estimated. For individual impacts, the error in this derived impact speed, due to uncertainties in the axes, eccentricities and inclinations of the ice grain's orbit, may be large, but is significantly reduced by considering larger ensembles of impacts – summing spectra within speed ranges.

In the laser-based analogue experiment, a liquid water beam and dissolved substances therein are primarily ionized by dispersion, a technique known as Laser Induced Liquid Beam Ion Desorption (LILBID)[39,40] (Figure 1 B). In this process, the energy transferred to the atoms and molecules by the laser is below their nominal ionization potentials, with the formation of charged species accomplished by mechanically breaking up the liquid matrix into charged fragments by laser excitation.[41,42] A similar mechanism may dominate the abundant cation formation from water ice grains at impact speeds as low as 3 km/s observed by Cassini's CDA. The dissociation energy of water (492.2 kJ/mol)[43] is under half its ionization energy (1183 kJ/mol)[44], which is less than that of H (1312 kJ/mol). It is therefore highly unlikely that significant quantities of $[H_3O]^+$ or $[H]^+$ ions can form by direct ionization at such low impact speeds.[42] Only at impact speeds > 15 km/s are charged water constituents from atomic/molecular collisional ionization observed, as we will demonstrate in this work. Mechanical breakage and collisional ionization almost exclusively produce spectra from singly-charged ions in both impact ionization and the laser desorption experiment. In space, the ionization process of water starts from solid ice whereas in the analogue experiment ionization occurs from the liquid phase.

While the mass resolution of CDA is a relatively low 20 – 50 (m/Δm)[31], SUDA's mass resolution reaches ≈ 200 m/Δm and the Enceladus Ice Analyzer (ENIA) is designed to achieve m/Δm > 1000.[32,33] With the current analogue experiment we are able to detect cations and anions with a mass resolution of about 800 m/Δm.

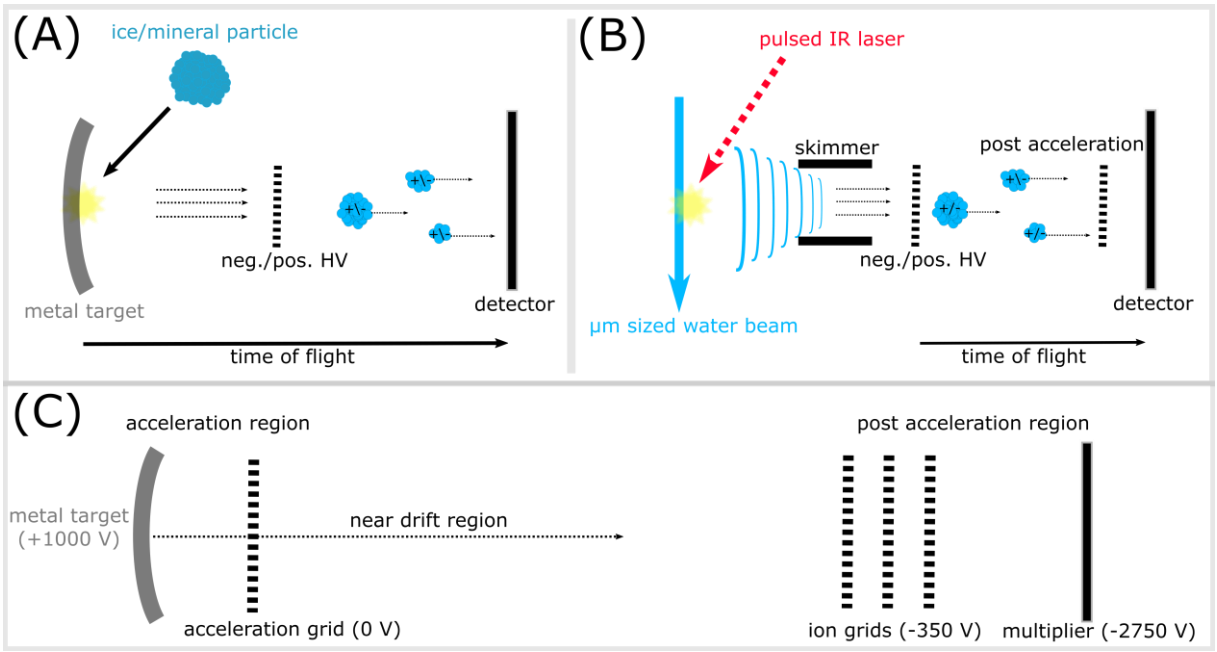

Figure 1: *Comparison of impact ionization with mass spectrometers in space (A) and liquid beam laser desorption (B) for comparable energy impact and dispersion conditions. In A) ice grains hit a metal target and become partially ionized. In B) a pulsed infrared laser hits a water beam, which disperses and in turn creates ions and charged aggregates. In both cases the charged ions/aggregates are accelerated by a high voltage potential difference (neg./pos. HV) and detected after a characteristic (mass/charge dependent) time of flight. The lower panel (C) shows the main acceleration and drift zones within the CDA Chemical Analyzer mass spectrometer. Voltages are approximate and the regions are not to scale. Instrument recording may be triggered by charges exceeding thresholds on the target, acceleration grids or multiplier.*

The aim of this work is to simulate, in the laboratory, impact ionization mass spectra arising from ice grains hitting a metal target at different impact speeds in space, by variation of both the laser's power density and the delay time of the gated mass spectrometer (see experimental description) to select fractions of the velocity distribution created by the desorption laser. We simulate spectra arising from the impacts of CDA Type 1 E ring ice grains. Type 1 grains are relatively homogeneous in their composition and are almost exclusively composed of water ice with occasional traces of sodium and potassium at the sub ppm level.[12,13] These grains are a population, as defined by the appearance of their CDA spectra, detected in Saturn's diffuse E ring.[12] Originating from Enceladus, the grains are believed to have formed via condensation and growth from water vapor expanding into space through fractures in Enceladus' surface.[12,45] CDA spectra of salt-rich (Type 3) ice grains are discussed in Postberg et al. 2009a, 2009b and 2011.[12,13,38] We therefore assume that the differences between CDA Type 1 spectra recorded at different impact speeds in Saturn's E ring are predominately due to kinetic effects rather than compositional differences. For each investigated speed regime (see below) we averaged over 12 – 20 individual spectra to further reduce the effects of minor compositional variations within Type 1 grains.

To cover the typical speed range of ice particles relevant for mass spectrometers in space, we examined representative Type 1 CDA mass spectra for five different impact speed regimes:

- 18 – 21 km/s
- 13 – 15 km/s
- 9 – 11 km/s
- 6.5 – 8.5 km/s

- 4 – 6 km/s

As previously mentioned, the impact speeds are determined by subtracting the known spacecraft speed from that of the ice grain, at the point of impact, calculated by assuming that the E ring grains are on circular orbits around Saturn. The natural distribution of orbital eccentricities and inclinations in the E ring will, however, introduce uncertainties in the exact impact speeds, which, as with minor compositional variation, are reduced by averaging over many spectra, over a suitably wide speed range.

To ensure a similar signal-to-noise ratio for all individual spectra at all speed regimes we used only those with an ion yield, as inferred from CDA's QI signal[31], of between 12 fC and 30 fC. In the E ring, CDA recorded many Type 1 spectra outside this range, mostly with lower ion yields. To ensure precise mass calibration of pure water peaks, Type 1 spectra with particularly low sodium and potassium signatures were selected.

Experimental description

Figure 2 shows the LILBID experimental setup used in Heidelberg and Leipzig as an analogue for ice grain impacts. An aqueous solution is injected into a high vacuum (5×10^{-5} mbar) through a quartz nozzle (opening radius 6 µm – 10 µm). The quartz nozzle is mounted on a three axis-manipulator and can be precisely adjusted. Flow injection of the tested solutions is accomplished with an injection valve (model MX9925, Rheodyne). An HPLC pump (model 300c, Gynkotek) is employed to keep the flow speed constant at 0.17 mL/min. The liquid flow is stable for ~ 2 mm vertically downward before disintegrating into droplets. To maintain the high vacuum, the liquid is captured by a nitrogen-cooled cryotrap. A second hanging nitrogen-cooled cryotrap freezes vaporized liquid. A pulsed infrared laser (Opolette HE 2731, OPOTEK; 20 Hz, 7 ns pulse length; maximum power density ≈ 1150 MW/cm^2) disperses the water beam. The laser, operating at a wavelength of 2840 nm (chosen to match the absorption frequency of the OH-stretch vibration of water) with a variable pulse energy of up to 4 mJ, is directed and focused onto the liquid through two CaF_2 lenses, a gold mirror and a CaF_2 window. When the water beam absorbs the laser energy, it is heated up and explosively disperses into atomic, molecular and macroscopic fragments.

After passing through a skimmer (a momentum separator resulting in a better-collimated spray of ions), cations or anions are analyzed in a reflectron-type Time-of-Flight mass spectrometer (TOF-MS; Kaesdorf).[16] The mass spectrometer operates at approximately 1 x

10^{-7} mbar and uses the principle of delayed extraction (Figure 2).[41] The spread in arrival times of the ions in the acceleration/extraction region, due to the field-free drift region (approximately 25 mm in length) between the site of ionization/dispersion and the acceleration region, is a function of the ions' initial velocities. Ion velocities are typically related to their masses and the amount of energy imparted by the laser (Equ. 1); a function not only of the maximum applied power density, but also distance away from the site of maximum power density along and through the liquid beam:

$$v_{ini} \sim \sqrt{\frac{E_{laser}}{m}} \qquad (1)$$

Within the extraction region itself, the effects of the ions' initial velocity dispersion are further reduced by variations in proximity to the extraction electrodes, with the fast ions having already passed through proportionally more of the extraction region prior to the electrode charging so that the fast ions experience less acceleration than the slow ions when the acceleration electrodes are switched on (Equ. 2):

$$U_{fast} < U_{slow} \qquad (2)$$

Samples of ions with defined ranges of initial velocities can thus be selected for analysis by the mass spectrometer. With delayed extraction, the acceleration electrodes (repeller and extractor) of the spectrometer are switched on after a predefined delay time for a duration of 30 µs. Late arriving ions are blocked by the repeller electrode and do not enter the MS because of the applied electrode potentials (Figure 2). Thus, by setting a delay time window this gated system selects ions dependent on their initial velocity. The delay time is defined by a pulse generator (model DG 535, Stanford Research Systems).

The detected (Photonis Chevron MCP-Set) signals are amplified (Preamp 100, Kaesdorf), digitized (12 bit, Acqiris) and then recorded with a LabVIEW controlled computer. Each mass spectrum presented here is the average of 500 individual spectra. NaCl solutions with concentrations of 1 x 10^{-7} M were used. The NaCl salt (purchased at Sigma Aldrich, p. a.) solutions are freshly prepared with doubly distilled and deionized H_2O in 50 mL sample cups. Performing one effective measurement requires a sample volume of ~ 0.5 mL.

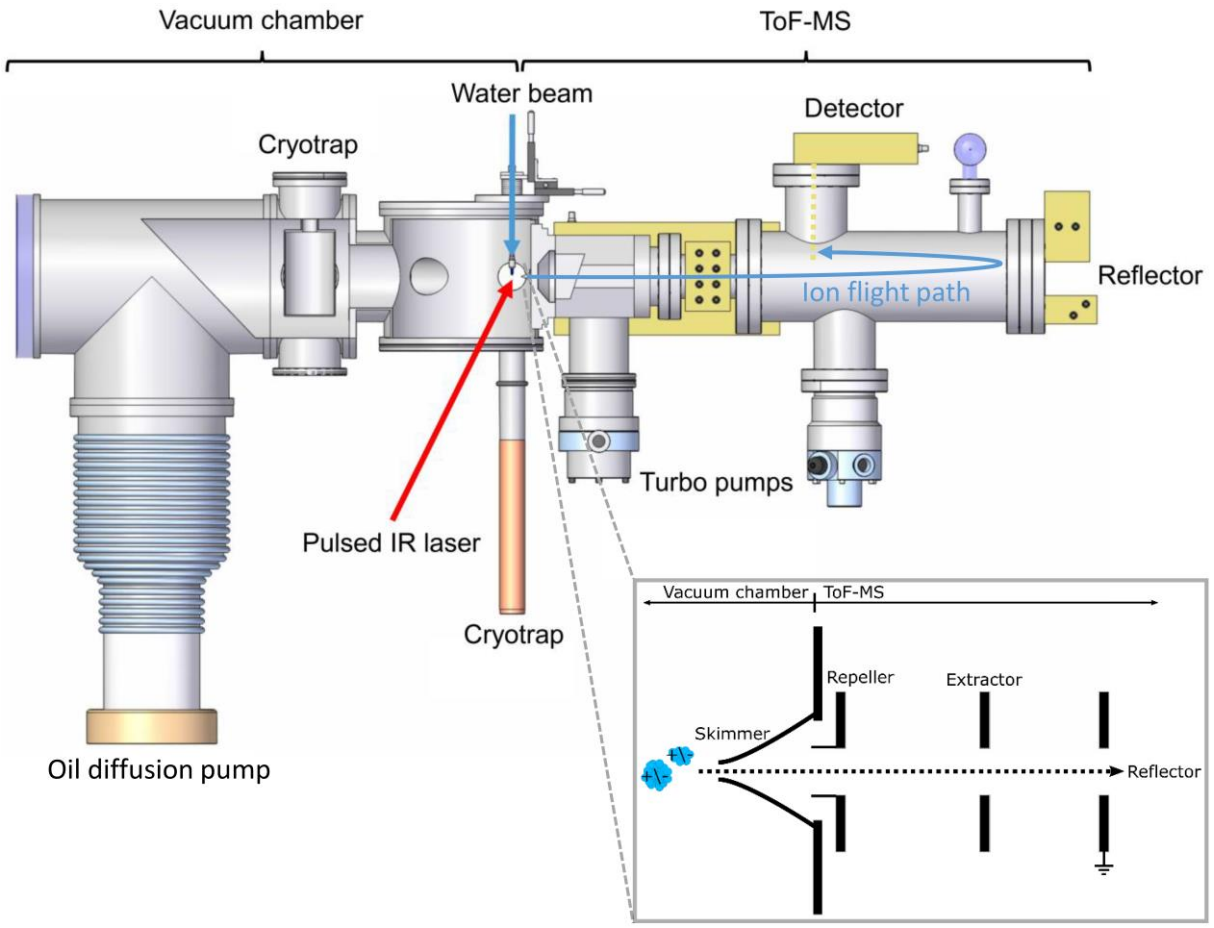

Figure 2: *Experimental LILBID-TOF-MS setup for simulating hypervelocity impacts of ice grains onto impact ionization mass spectrometers in space and (inset) a schematic illustrating the instrument configuration underlying the principle of delayed extraction. The start signal occurs when the acceleration electrodes are switched on, the stop signal when the ions reach the detector. The oil diffusion pump shown was later replaced by a turbo pump (adapted from Postberg et al. 2018).*[14] *See text for further explanation.*

3 Results

CDA Type 1 spectra characteristics at different speed regimes

The averaged CDA Type 1 spectra for each speed regime used in this work are shown in Figure 3. At below 15 km/s they show peaks of pure water clusters with masses corresponding to $[(H_2O)_nH_3O]^+$ (n = 0, 1, 2…). The averaged spectra exhibit a general amplitude maximum at n = 0 and a monotonous decline from small to large n, although in some individual spectra the maximum is reached at n = 1, 2 or 3 at low and intermediate speeds (≤ 10 km/s). The lower the impact speed and, therefore, the kinetic energy of the

impact (assuming equally-sized ice grains) the more abundant are water clusters with larger n. Because the ice grains contain traces of sodium and potassium, originally probably in the form of NaCl and KCl[12], the averaged mass spectra for all speed regimes also show peaks due to sodium water clusters $[(H_2O)_nNa]^+$ and potassium water clusters $[(H_2O)_nK]^+$. Owing to the insufficient mass resolution of CDA, the water cluster peaks of the three different charge bearing species $[H_3O]^+$, $[K]^+$ and $[Na]^+$ overlap at 19u $(+18u)_{n+1}$, 39u $(+18u)_n$, and 23u $(+18u)_{n+1}$. Because of the dominant pure water cluster peaks ($[(H_2O)_nH_3O]^+$), $[Na]^+$ and $[K]^+$ cluster peaks are often not quantifiable. CDA's target material rhodium is excavated and detectably ionized at impact speeds > 9 km/s[38] and thus $[Rh]^+$ ion signatures are apparent in the three fastest speed regimes in the form of $[Rh]^+$, rhodium dimers $[Rh_2]^+$ and rhodium water clusters $[(H_2O)_{1-4}Rh]^+$.

In CDA spectra of the two fastest speed regimes recorded, above ≈ 13 km/s, $[H]^+$, $[H_2]^+$ and $[H_3]^+$ are created and above ≈ 15 km/s ions typical for dissociation and ionization of water molecules ($[OH]^+$, $[OH_2]^+$, $[O]^+$, $[O_2]^+$) start to appear, whereas any water clusters with $n \geq 1$ start to disappear and are undetectable at ≥ 20 km/s.

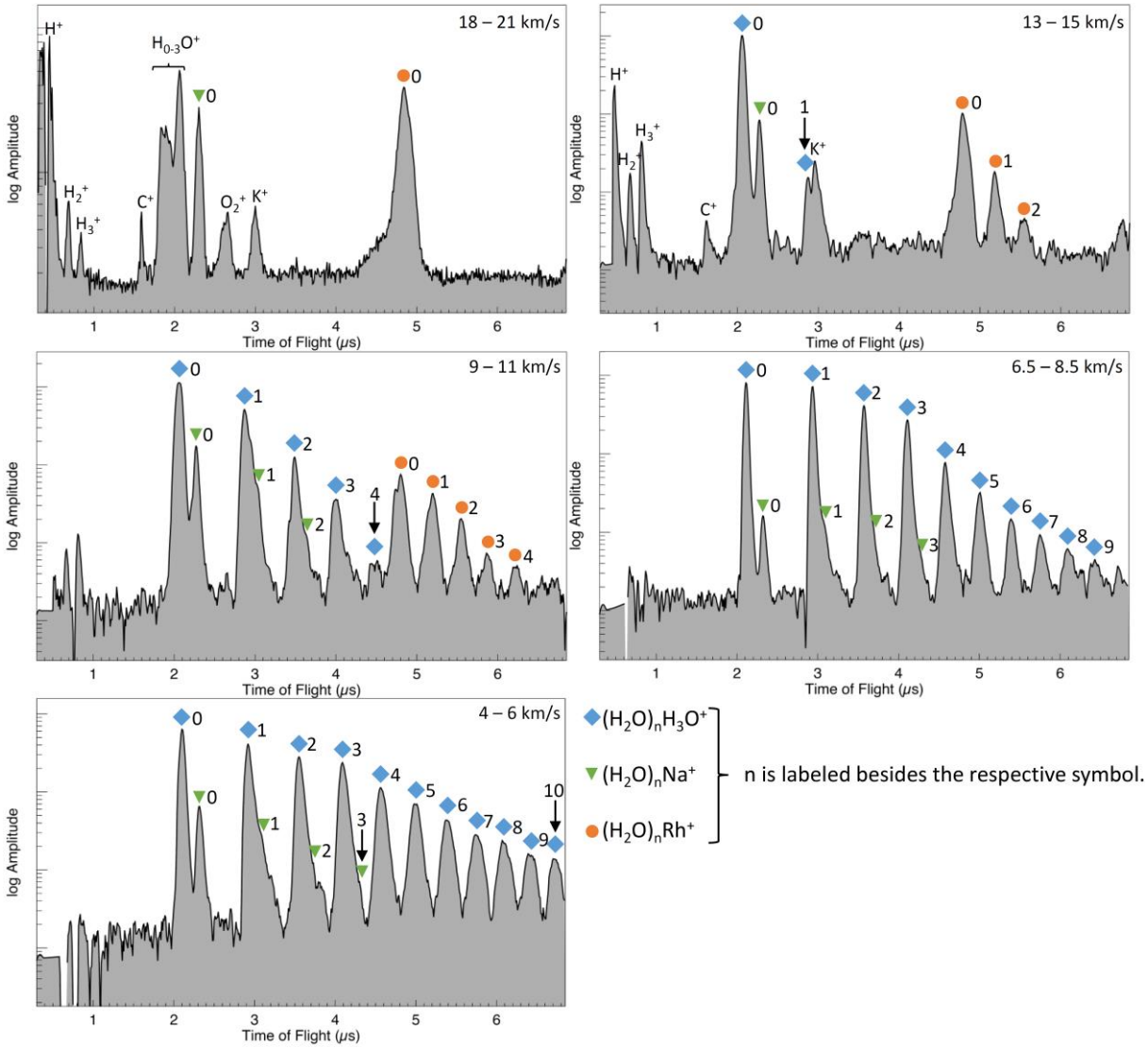

Figure 3: *Baseline corrected CDA mass spectra of ice grains at different impact speeds. At the fastest impact speeds (18 – 21 km/s) hydronium $[(H_2O)H]^+$ (19u) and elemental $[Na]^+$ (23u) and $[K]^+$ peaks (39u) are observable, whereas no molecular water cluster peaks are detectable. Here dissociation ions are formed from the water molecules, due to the high kinetic energy of the impinging ice grains: Water molecules disintegrate forming hydrogen $[H]^+$ (1u), dihydrogen $[H_2]^+$ (2u), trihydrogen $[H_3]^+$ (3u), oxygen $[O]^+$ (16u), hydroxyl $[HO]^+$ (17u), water $[H_2O]^+$ (18u), and dioxygenyl $[O_2]^+$ (32u) cations. At 13 – 15 km/s, detectable quantities of molecular dissociation ions do not form and water clusters $[(H_2O)_nH_3O]^+$ with n = 0 and n = 1 are observable. At 9 - 11 km/s larger pure water clusters are detected at least up to n = 4 (91 u) and water sodium clusters up to n = 2 (59u), respectively. Due to CDA's relatively low mass resolution, with increasing n the K and Na clusters are increasingly difficult to separate from the adjacent pure water clusters and thus might not be identified if present in small quantities. At ≈ 8 km/s pure water clusters usually extend to n ≥ 7 and below 6 km/s water clusters are frequently observable up to the end of*

CDA's mass range of about 200 u (n ≥ 10). The amplitudes of the pure water cluster peaks and the sodium water cluster peaks decline from lower to higher masses in CDA spectra at all speed regimes. The sequence of nearly exponentially declining amplitudes is interrupted by a "jump" between water clusters with n = 3 and n = 4. This is due to the well-known "magic number" stability of n = 3 water clusters.[46,47] *Above 9 km/s* $[(H_2O)_nRh]^+$ *clusters are frequently observable. The number of water molecules attached to* $[Rh]^+$ *typically corresponds to the number of water molecules in the pure water cluster cation. For example in the spectrum of 13 – 15 km/s two water molecules are attached to rhodium (*$[(H_2O)_2Rh]^+$*) and the largest pure water cluster in the spectrum consist of a protonated cluster of two water molecules* $[(H_2O)H_3O]^+$.

Reproducing CDA Type 1 spectra with the analogue experiment

We aim to reproduce the speed-dependent occurrence of water cluster and atomic ions with the laboratory setup, such that both the overall spectral envelope (pattern of peak amplitudes) and appearance and disappearance (within instrument detectability thresholds) of molecular and atomic species are simulated. We use a highly diluted NaCl solution (see Experimental section) without potassium salts and thus K cluster peaks are absent in the analogue spectra, as are Rh-based peaks from the CDA target material. To simulate the fastest two impact speed regimes (18 – 21 km/s and 13 – 15 km/s) a single delay time window at a short delay time, to extract the fastest ions, is sufficient to reproduce CDA spectra. For the next slower speed regime (9 – 11 km/s) further spectra taken at a longer delay time have to be added to a "fast ion" window as used for 18 – 21 km/s and 13 – 15 km/s. For the slowest two speed regimes (6.5 – 8.5 km/s and 4 – 6 km/s) a third delay time window at even longer delay times has to be added. In the impact ionization process, ionization and disruption of the water ice grains occur *within* the acceleration region of the instrument. However, the laboratory laser experiment generates ions in a field-free zone, which then drift into the acceleration region. The apparent production time of the ions is therefore significantly extended, requiring selection (via delay times of the gating system) of ion populations to match those seen in impact ionization experiments. Co-added spectra produced from a mixture of different delay time windows are therefore generated with the LILBID setup (see also Discussion). The following energy densities and delay times have been used to match the peak patterns produced in the different CDA impact speed regimes:

- 18 - 21 km/s: 1150 MW/cm^2 and 4.4 µs

- 13 – 15 km/s: 975 MW/cm^2 and 3.2 µs
- 9 – 11 km/s: 975 MW/cm^2 and 3.8 µs added to 670 MW/cm^2 and 4.9 µs
- 6.5 – 8.5 km/s: 975 MW/cm^2 and 3.8 µs added to 670 MW/cm^2 and 4.9 µs added to 540 MW/cm^2 and 5.7 µs
- 4 – 6 km/s: 975 MW/cm^2 and 3.8 µs added to 670 MW/cm^2 and 4.9 µs added to 445 MW/cm^2 and 6.3 µs

Figure 4 shows the reproduced CDA spectra resulting from the analogue experiment. Despite the different aggregate states of water, solid in space and liquid in the laboratory, very similar cation mass spectra are produced (Figures 3 and 4).[12,28] The higher mass resolution of the latter is clearly observable. Peak patterns can be reproduced accurately for impact speeds up to 15 km/s. In the regime above 18 km/s all ion species can be reproduced but with a poorer quantitative match. Table 1 shows a comparison of the relative amplitude ratios of water peaks in CDA spectra with laboratory spectra for impact speeds up to 15 km/s.

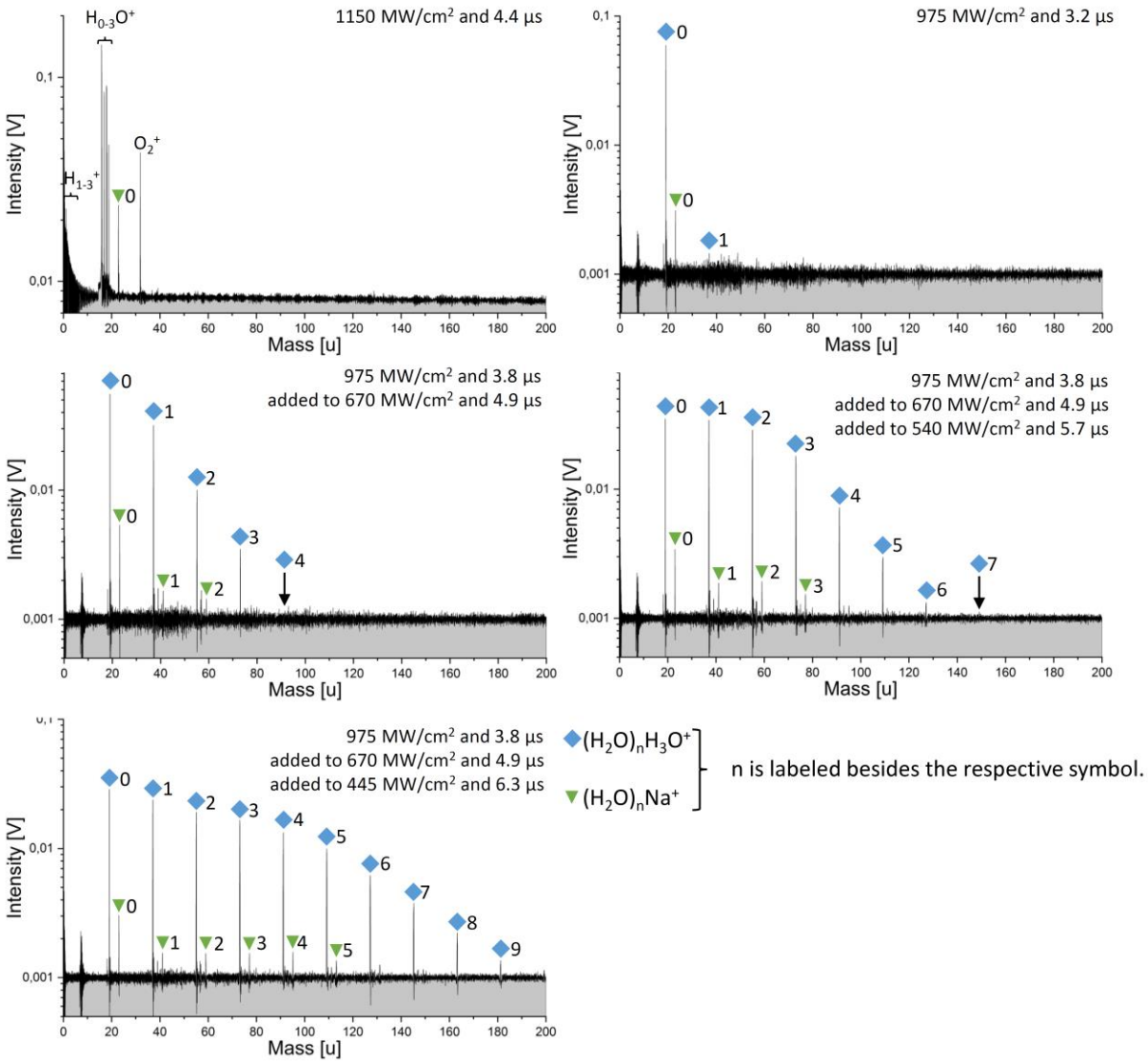

Figure 4: *Baseline corrected laboratory analogue spectra of CDA Type 1 spectra for 5 different speed regimes (Figure 3). The panel's positions correspond to the panels in Figure 3. A solution of 10^{-7} M NaCl was used to match the sodium content of the selected Type 1 ice grains. In both CDA spectra and laboratory spectra identical ion species are observable in similar quantities.*

4 Discussion

We have shown that it is possible to recreate the effects of impact speed on the impact ionization mass spectra of micron and sub-micron Type 1 E ring ice grains using a laboratory LILBID apparatus. In order to determine salt concentrations within the grains, other Type 1 spectra have been reproduced previously with similar LILBID-MS experiments using a solution of 10^{-6} M NaCl.[12] Here we find somewhat lower concentrations of 1 x 10^{-7} M yield

spectra which better agree with those of the selected Type 1 E ring grains, which were biased towards particularly low sodium and potassium contents, in order to rule out resolution-limited, isobaric, peak interference effects in the water cluster peaks in CDA spectra (see Experimental section).

The different phases of water, solid in space and liquid in the laboratory experiment, do not make a noticeable difference to the resulting cation spectra and very similar ensembles of molecular and elemental cations are created, as has also been shown for liquid water and ice in the LILBID approach.[28,48] The energies required for dispersion of the liquid to form ions and charged aggregates for a given number of molecules (1183 kJ/mol) far exceed the energies required for phase transitions in the H_2O system (vaporization energy of water at 0 °C is 45 kJ/mol). The main difference in spectral appearance comes from the higher resolution of the reflectron MS used in the laboratory.

There are two processes through which $[(H_2O)_nH]^+$ ions can form in impact clouds or during the LILBID process. The first, for which evidence has been presented by e.g. Wiederschein et al. (2015) for LILBID, is via direct formation of charged fragments.[42] Upon dispersion of a water beam, statistical inhomogeneities in the distribution of charges result in excesses of charges on some fragments. This process does not create abundant $[H]^+$ ions (Fig. 4). The impinging laser generates a shock wave in the water beam, which travels at approximately 2 km/s.[49] This is analogous to the shock wave generated during the impact of an ice grain onto a metal target, although in this latter case a fraction of the available energy is also transferred to the target.[29]

Given the lack of $[H]^+$ ions in the CDA spectra at low (< 9-11 km/s) speeds (Fig. 3), together with the arguments based on impact energies (and speed thresholds) discussed previously (Experimental section), it is likely that ion formation in impact clouds generated by low speed ice grains occurs by the same mechanism, a "top down" dispersion/fragmentation process for molecular ion production.[42]

However, with increasingly energetic conditions, and shorter lifetimes, impact clouds from higher speed (> 9-11 km/s) impacts show evidence that clustering, forming larger molecular assemblages from a "bottom up" approach, is occurring as well. The definite clusters, in this instance, are between the target material, Rh, and both hydronium and larger water clusters/fragments. At similar speeds, $[H]^+$ appears in the spectra, preceded at slightly lower speeds by appearance of $[H_2]^+$ and $[H_3]^+$, although it is probable that the hydrogen is, in these cases, also released from the Rh target, in which significant amounts are absorbed.[38] The

impact cloud is therefore an environment in which collisional growth can occur, and this process, in addition to fragmentation, is likely to form clusters of water molecules.

Cluster growth is related to the likelihood of ions, or neutrals, encountering other molecules, as the timescale over which suitable conditions exist. It is therefore a function of the number density of neutrals and ions within the impact cloud, together with their size and speed distributions. These will change with time, as the impact cloud expands and clustering (or fragmentation and/or dissociation) occurs. The initial number density of neutrals and ions, and the expansion rate of the impact cloud, are related to the impact conditions, in particular particle mass and impact speed. Of these, impact speed is the dominant characteristic, with the energy density of the impact scaling with kinetic energy, and the total charge generated proportional to $m^{\alpha}v^{\beta}$, where α is typically 1 and β is typically 3-5, depending on particle composition.[27,30]

In the impact process, with increasing energy densities, molecular dissociation and the formation of atomic (and molecular fragment) ions starts to occur. In the LILBID process, the individual photon energy (6.99 x 10^{-20} J) is too low to directly dissociate the HO-H bond in water (8.19 x 10^{-18} J) or ionize atomic H (2.18 x 10^{-18} J). However, with increasing laser power density in the LILBID experiments, the charge density and dispersion speed of the vapor cloud will increase, mimicking the impact plasma shockwave and cloud expansion, until molecular dissociation and ionization of the water molecules starts to occur, primarily through collisional processes, leading to the formation of a cationic plasma component composed of e.g. $[H]^+$, $[H_2]^+$, $[H_3]^+$, $[O]^+$, $[O_2]^+$, $[OH]^+$ and $[H_2O]^+$, species dominating CDA spectra above approximately 18 km/s. It is indeed typical, that the generation of such ions only occurs above specific speed thresholds in impact ionization at which the localized energy density at the impact site becomes high enough.[37] At the lower impact speeds the slow expansion speed, and hence longer impact cloud lifetime, increase the likelihood of any minor $[H]^+$ component clustering, potentially resulting in the same lack of $[H]^+$ that would be seen if fragmentation dominated. For the Type 1 E ring grains, the threshold at which the spectra become dominated by dissociated water ions, and large water clusters become undetectable, is approximately 18 km/s.

Below 15 km/s, by choosing the appropriate delay time windows, a near quantitative match between laboratory and flight spectra can be achieved (Table 1). In contrast, the decisive difference between the two fastest speed regimes is the applied laser energy, such that the plasma is either dominated by dissociated atomic or molecular fragment ions (>18 km/s), or

stays in the regime where spectra are dominated by larger molecular ions (<15 km/s). The sudden difference in plasma behavior between these two regimes in the LILBID experiment results in a reduced signal to noise if short delay times are used, and hence a longer (4.4 μs) time was selected to maximize the spectral signal. In fact, in general the reproduction of CDA spectra is more difficult in the dissociation regime. While all ion species seen in CDA spectra still show up in the analogue experiment, the quantitative match is worse and ion abundances in the dissociation regime are generally much more variable in both CDA spectra and laboratory spectra. There is a general trend that $[H_{1,2,3}]^+$ and $[H_3O]^+$ form in larger abundances in high speed impact ionization spectra whereas $[O]^+$, $[HO]^+$, $[H_2O]^+$ and $[O_2]^+$ are overrepresented in the laboratory spectra.

Theoretical investigations of the impact ionization process, considering Fe particles impacting metal targets, indicate that at speeds lower than 20 km/s at most ~10-15% of the particles is ionized and does not recombine prior to detection[50], with the majority of the particle remaining neutral, or even in macroscopic fragments. This is likely to also be the case with the water ice grains. In the LILBID experiments, the approx. 100 micron wide gaussian laser power density profile, together with the significant vertical (and horizontal in comparison with the typical size of Type 1 E ring grains) extension of the water beam, will result in a similar variation in energy transfer and ion formation. This issue can be partially overcome by e.g. shooting on individual water droplets, but this method yields highly irreproducible results with our experimental setup. Reducing the length of the water beam by using on-demand nozzles has had some success in mitigating this problem[51] although here we correct for it by the use of appropriate delay time windows.

It is important to note that the measured composition of the impact plasma, and that of the LILBID plasma, is that produced before a "steady state", has been reached via thermalisation, with the ion ensemble also having undergone subsequent evolution (e.g. recombination, collisional clustering and fragmentation) during the acceleration/drift periods. Apart from population differences arising from e.g. the extent of the water beam, the main difference between the ion ensembles detected from impact ionization and those arising from the LILBID experiment is due to differences in the electric field environment in which ionization and molecular cluster/fragment formation occurs (imposed by the use of liquid in the LILBID apparatus). Within the CDA, generated ions are collected and accelerated rapidly towards the ion detector (multiplier) as soon as any Debye shielding breaks down and the ions are exposed to the 330 kV/m electric field.[31] In the LILBID apparatus, ions drift through a completely field-free region after production, prior to entering the mass spectrometer for subsequent

acceleration and detection. The speed at which the ions traverse this region is analogous to the speed with which the impact cloud expands, with faster ions having been exposed to the highest energy densities in the water beam. As with impact ionization, these ions tend to have undergone greater fragmentation, less clustering, or even undergone dissociation. Conversely, ions which are slow to traverse the LILBID drift region are larger and less fragmented (or more clustered, with reduced, thermalized speeds). To simulate the short "snapshot" of the impact plasma sampled by CDA, it is therefore necessary to generate and select suitable populations of ions which have undergone similar energetic conditions in the LILBID experiment. This is achieved by combining variations in laser power density with use of the aforementioned delay time windows.

5 Conclusion and outlook

The LILBID laboratory experiment is capable of successfully reproducing impact ionization mass spectra generated by micron- and sub-micron-sized icy dust grains impinging onto spaceborne mass spectrometers over a wide range of impact speeds. The mass spectra of Type 1 ice grains recorded by Cassini's CDA mass spectrometer at impact speeds ranging from 4 to 21 km/s can be reproduced using LILBID-MS by the selection of appropriate laser and ion extraction parameters. The shorter the delay time and the higher the laser's power density, the higher the simulated impact speed.

The experimental settings inferred from comparison of this simple spectrum type that match the different speed regimes can now be applied to more complex spectra. Future work will extend these results to produce an accurate speed- and matrix-dependent analysis of CDA salt-rich Type 3 mass spectra. Type 3 mass spectra show characteristic mass spectral features arising from high concentrations of sodium salts (0.5-2% by mass).[12,13] Earlier work[12] with a similar analogue experiment successfully reproduced co-added CDA Type 3 spectra produced by averaging over a large number of individual impact events but did not consider the effects of considerable variations in grain impact speeds. Compared to Type 1 grains, Type 3 grains bear sodium and potassium salts at much higher concentrations and are thought to be aerosolized samples of Enceladus' subsurface ocean water.[12,13] In a similar way we can now also investigate the composition of organic-bearing Type 2 ice grains emitted by Enceladus[10,11,14], which show characteristic mass spectral features arising from organic compounds, over a wide range of different impact speeds recorded by CDA, giving access to different, speed dependent spectral fragmentation patterns of the organic molecules.

The broader general goal is to establish a high resolution, bipolar (cation and anion), spectrum library, covering a large sample of organic and inorganic compounds in a water matrix, applicable to future spaceborne impact ionization mass spectrometers. Because the ionization process is intimately linked to the impact speed, spectral appearance is a function not only of composition but also of impact speed. With this work we have established a standard methodology for the laboratory reproduction of spectra over a wide range of impact speeds, which can be applied to the generation of a spectrum library.

Acknowledgements

We thank Lenz Nölle and Zenghui Zou for valuable discussions. We acknowledge the work of the scientists and engineers of the Cassini team. The research leading to these results received financial support from the German Research Foundation (DFG) projects PO 1015/2-1, /3-1, /4-1, project AB 63/9-1, and ERC Consolidator Grant 724908-Habitat OASIS.

References

[1] Berg OE, Richardson FF. The Pioneer 8 Cosmic Dust Experiment. *Rev Sci Instruments.* 1969;40:1333-1337.

[2] Brownlee DE, Burnett D, Clark B, et al. STARDUST: comet and interstellar dust sample return mission. Physics, Chemistry, and Dynamics of Interplanetary Dust, 150th Colloquium of the International Astronomical Union. B. A. S. Gustafson, M. S. Hanner, ed. Astronomical Society of the Pacific Conference Series, San Francisco, Gainesville, Florida; 1995:223-226.

[3] Drolshagen G, Svedhem H, Grün E, Bunte KD. Measurements of cosmic dust and micro debris in GEO. *Adv Space Res.* 2001;28:1325-1333.

[4] Grün E, Fechtig H, Giese RH, et al. The Ulysses dust experiment. *Astron Astrophys.* 1992;92:411-423.

[5] Grün E, Fechtig H, Hanner MS, et al. The Galileo dust detector. *Space Sci Rev.* 1992;60:317-340.

[6] Kissel J, Sagdeev RZ, Bertaux JL, et al. Composition of Comet Halley dust particles from Vega observations. *Nature.* 1986;321:280-282.

[7] Hillier JK, Green SF, McBride N, et al. The composition of Saturn's E ring. *Mon Not R Astron Soc.* 2007;377:1588-1596.

[8] Hsu H-W, Postberg F, Sekine Y, et al. Ongoing hydrothermal activities within Enceladus. *Nature.* 2015;519:207-210.

[9] Kempf S, Beckmann U, Moragas-Klostermeyer G, et al. The E-ring in the vicinity of Enceladus I. Spatial distribution and properties of the ring particles. *Icarus.* 2008;193:420-437.

[10] Khawaja N, Postberg F, Hillier J, et al. Low mass nitrogen-, oxygen-bearing and aromatic compounds in Enceladean ice grains. *Mon Not R Astron Soc.* 2019 (in press).

[11] Postberg F, Kempf S, Hillier JK, et al. The E-ring in the vicinity of Enceladus II. Probing the moon's interior–The composition of E-ring particles. *Icarus.* 2008;193:438-454.

[12] Postberg F, Kempf S, Schmidt J, et al. Sodium salts in E-ring ice grains from an ocean below the surface of Enceladus. *Nature.* 2009a;459:1098-1101.

[13] Postberg F, Schmidt J, Hillier J, Kempf S, Srama R. A salt-water reservoir as the source of a compositionally stratified plume on Enceladus. *Nature.* 2011a;474:620-622.

[14] Postberg F, Khawaja N, Abel B, et al. Macromolecular organic compounds from the depth of Enceladus. *Nature.* 2018;558:564-568.

[15] Tobie G. Enceladus' hot springs. *Nature.* 2015;519:162-163.

[16] Mamyrin BA. Laser assisted reflectron time-of-flight mass spectrometry. *Int J Mass Spectrom*. 1993;131:1-19.

[17] Balsiger H, Altwegg K, Bochsler P, et al. ROSINA – Rosetta Orbiter Spectrometer for Ion and Neutral Analysis. *Space Sci Rev.* 2007;128:745-801.

[18] Barabash S, Wurz P, Brandt P, et al. Particle Environment Package (PEP). *European Planetary Science Congress* 2013;8:EPSC2013-709.

[19] Waite JH, Lewis WS, Kasprzak WT, et al. The Cassini Ion and Neutral Mass Spectrometer (INMS) Investigation. *Space Sci Rev.* 2004;114:113-231.

[20] Timmermann R, Grün E. Plasma emission from high velocity impacts of microparticles onto water ice. Origin and Evolution of Interplanetary Dust. Levasseur-Regourd AC and Hasegawa H, ed. 1991:375–378.

[21] Burchell MJ, Cole MJ, McDonnell JAM, Zarnecki JC. Hypervelocity impact studies using the 2 MV Van de Graaff accelerator and two-stage light gas gun of the University of Kent at Canterbury. *Meas Sci Technol.* 1999;10:41-50.

[22] Fielding LA, Hillier JK, Burchell MJ, Armes SP. Space science applications for conducting polymer particles: synthetic mimics for cosmic dust and micrometeorites. *Chem Commun.* 2015;51:16886-16899.

[23] Goldsworthy BJ, Burchell MJ, Cole MJ, et al. Time of flight mass spectra of ions in plasmas produced by hypervelocity impacts of organic and mineralogical microparticles on a cosmic dust analyser. *Astron Astrophys.* 2003;409:1151-1167.

[24] Hasegawa S, Hamabe Y, Fujiwara A, et al. Microparticle acceleration for hypervelocity experiments by a 3.75MV Van de Graaff accelerator and a 100kV electrostatic accelerator in Japan. *Int J Impact Eng.* 2001;26:299-308.

[25] Mocker A, Armes A, Bugiel S, et al. The Heidelberg Dust Accelerator: Investigating Hypervelocity Particle Impacts. *American Geophysical Union, Fall Meeting;* 2010:P31B-1524.

[26] Shu S, Collette A, Drake K, et al. 3 MV hypervelocity dust accelerator at the Colorado Center for Lunar Dust and Atmospheric Studies. *Rev Sci Instruments.* 2012;83:075108.

[27] Stübig M. New insights in impact ionization and in time-of-flight mass spectroscopy with micrometeoroid detectors by improved impact simulations in the laboratory. *Dissertation* Ruprecht-Karls-Universität Heidelberg; 2002.

[28] Beinsen A. Bildgebung und chemische Analytik mit Laserdesorptions-Massenspektrometrie im Bereich Forensik und Astrophysik. *Dissertation* Georg-August-Universität Göttingen; 2011.

[29] Hornung K, Kissel J. On shock-wave impact ionization of dust particles. *Astron Astrophys.* 1994;291:324-336.

[30] Bedford DK. Impact ionization of micro-particles at low velocities. *J Phys A.* 1971;4:L14-L18.

[31] Srama R, Ahrens TJ, Altobelli N, et al. The Cassini Cosmic Dust Analyzer. *Space Sci Rev.* 2004;114:465-518.

[32] Kempf S, Srama R., Grün E, et al. Linear high resolution dust mass spectrometer for a mission to the Galilean satellites. *Planet Space Sci.* 2012;65:10-20.

[33] Reh K, Cable ML, Clarke K, et al. Enceladus Life Finder: The Search for Life in a Habitable Moon. *IEEE Aerospace Conference*; 2016:1-8.

[34] Postberg F, Grün E., Horanyi M, et al. Compositional Mapping of Planetary Moons by Mass Spectrometry of Dust Ejecta. *Planet Space Sci.* 2011b;59:1815-1825.

[35] Mitri G, Postberg F, Soderblom JM, et al. Explorer of Enceladus and Titan (E 2 T): Investigating ocean worlds‘ evolution and habitability in the solar system. *Planet Space Sci.* 2018;155:73-90.

[36] Lunine J, Waite H, Postberg F, et al. Enceladus life finder: the search for life in a habitable moon. EGU General Assembly Conference Abstracts 2015;17.

[37] Fiege K, Trieloff M, Hillier JK, et al. Calibration of relative sensitivity factors for impact ionization detectors with high-velocity silicate microparticles. *Icarus.* 2014;241:336-345.

[38] Postberg F, Kempf S, Rost D, et al. Discriminating contamination from particle components in spectra of Cassini’s dust detector CDA. *Planet Space Sci.* 2009b;57:1359-1374.

[39] Karas M, Glückmann M, Schäfer J. Ionization in matrix-assisted laser desorption/ionization: singly charged molecular ions are the lucky survivors. *J Mass Spectrom.* 1988;35:1-12.

[40] Karas M, Bahr U, Ingendoh A, et al. Principles and applications of matrix-assisted UV-laser desorption/ionization mass spectrometry. *J Chromatogr B.* 1991;562:745-746.

[41] Charvat A, Abel B. How to make big molecules fly out of liquid water: applications, features and physics of laser assisted liquid phase dispersion mass spectrometry. *Phys Chem Chem Phys.* 2007;9:3335-3360.

[42] Wiederschein F, Vöhringer-Martinez E, Beinsen A, et al. Charge separation and isolation in strong water droplet impacts. *Phys Chem Chem Phys.* 2015;17:6858-6864.

[43] Maksyutenko P, Rizzo TR, Boyarkin OV. A direct measurement of the dissociation energy of water. *J Chem Phys*. 2006;125:181101.

[44] Kovtun YV. Mean energy of water molecule ionization by electron impact. *Tech Phys*. 2015;60:1110-1118.

[45] Schmidt J, Brilliantov N, Spahn F, Kempf S. Slow dust in Enceladus‘ plume from condensation and wall collision in tiger stripe fractures. *Nature.* 2008;451:685-688.

[46] Andersson PU, Ryding MJ, Sekiguchi O, Uggerud E. Isotope exchange and structural rearrangements in reactions between size-selected ionic water clusters, $H_3O^+(H_2O)_n$ and $NH_4^+(H_2O)_n$, and D_2O. *Phys Chem Chem Phys.* 2008;10:6127-6134.

[47] Niedner-Schatteburg G, Bondybey VE. FT-ICR Studies of Solvation Effects in Ionic Water Cluster Reactions. *Chem Rev.* 2000;100:4059-4086.

[48] Berkenkamp S, Karas M, Hillenkamp F. Ice as a matrix for IR-matrix-assisted laser desorption/ionization: Mass spectra from a protein single crystal. *Proc. Natl. Acad. Sci USA* 1996;93:7003-7007.

[49] Charvat A, Stasicki, B, Abel B. Product screening of fast reactions in IR-laser-heated liquid water filaments in a vacuum by mass spectrometry. *J Phys Chem A.* 2006;110:3297-3306.

[50] Drapatz S, Michel KW. On the intensity of rotational lines of H_2 and HD from dense interstellar clouds. *Astron Astrophys.* 1974;36:211-216.

[51] Morgner N, Barth H-D, Brutschy BA. New Way to Detect Noncovalent Bonded Complexes of Biomolecules from Liquid Micro-Droplets by Laser Mass Spectrometry. *Aust. J. Chem.* 2006;59:109-114.

Table 1: A *comparison of relative water peak amplitude ratios (normalized to the 19 u signal) of the co-added CDA mass spectra (Figure 3) at different impact speeds with laboratory results (Figure 4). All peaks apparent in CDA mass spectra are also seen in the laboratory mass spectra, with a near quantitative match of the relative amplitude ratios achieved.*

Impact speed [km/s]	**mass [u]**	19	37	55	73	91	109	127	145	163	181	199
13 – 15	**CDA**	100	1.7	-	-	-	-	-	-	-	-	-
	lab	100	2.4	-	-	-	-	-	-	-	-	-
9 – 11	**CDA**	100	51.0	15.7	4.6	0.7	-	-	-	-	-	-
	lab	100	56.4	15.3	5.6	2.1	-	-	-	-	-	-
6.5 – 8.5	**CDA**	100	92.6	50.6	35.2	8.0	3.1	1.5	1.0	-	-	-
	lab	100	90.1	68.1	32.7	11.6	5.4	3.1	2.8	-	-	-
4 – 6	**CDA**	100	60.6	44.7	34.8	17.4	12.2	7.6	4.7	3.6	2.7	1.8
	lab	100	64.7	39.2	26.0	21.2	16.2	10.4	6.7	4.5	3.1	2.8